

Effect of Preparation Methods on the Physicochemical and Functional Properties of Ni/CeO₂ Catalysts

E. V. Matus^{a,b,*}, A. S. Shlyakhtina^{a,b}, O. B. Sukhova^a, I. Z. Ismagilov^a, V. A. Ushakov^a, S. A. Yashnik^a,
A. P. Nikitin^c, P. Bharali^d, M. A. Kerzhentsev^a, and Z. R. Ismagilov^{a,c}

^a*Boreshkov Institute of Catalysis, Siberian Branch, Russian Academy of Sciences, Novosibirsk, 630090 Russia*

^b*Novosibirsk State Technical University, Novosibirsk, 630073 Russia*

^c*Institute of Coal Chemistry and Material Science FRS CCC, Siberian Branch,
Russian Academy of Sciences, Kemerovo, 650000 Russia*

^d*Tezpur University, Napaam, Tezpur, 784 028 Assam, India*

**e-mail: matus@catalysis.ru*

Received November 29, 2018; revised November 29, 2018; accepted November 29, 2018

Abstract—The effect of preparation procedures (a polymer ester precursor method and incipient wetness impregnation) on the physicochemical and functional properties of Ni/CeO₂ catalysts with different nickel contents (0–15 wt %) was studied in order to develop highly active and carbonization-resistant catalysts for hydrocarbon reforming. Based on the results of studying the samples by low-temperature nitrogen adsorption, X-ray phase analysis, Raman spectroscopy, transmission electron microscopy and temperature-programmed reduction with hydrogen, it was found that the textural, structural, and redox properties of the materials depend on the method of their synthesis. As compared with the samples prepared by impregnation, the Ni/CeO₂ catalysts obtained by the polymer ester precursor method were characterized by different active component stabilization forms (a Ce_{1-x}Ni_xO_y solid solution phase and NiO particles <5 nm in size vs. a NiO phase with a particle size of 5–50 nm), a smaller average size of CeO₂ crystallites (5.5 vs. 11 nm), a high specific surface area (105 vs. 75 m²/g), a defect structure, and a decreased reducibility. It was found that the samples of both series provided comparable yields of hydrogen (to 50% at 600°C) in an autothermal ethanol reforming reaction, but the Ni/CeO₂ catalysts synthesized by the polymer ester precursor method were more resistant to the formation of carbonaceous deposits.

Keywords: Ni catalysts, cerium dioxide, preparation method, ethanol, reforming

DOI: 10.1134/S002315841902006X

INTRODUCTION

Cerium dioxide is widely used in catalysis as an active component, support, or modifying additive [1–5]. The stability of the fluorite-type cubic structure of nonstoichiometric cerium dioxide and the presence of the Ce⁴⁺/Ce³⁺ redox pair are responsible for the advantages of using systems based on it. The properties of this material are unique due to the high oxygen capacity and the mobility of crystal lattice oxygen, the ability to form Ce_{1-x}M_xO_y solid solutions of various compositions (M = Zr, La, Pr, Gd, Y, Mg, etc.), and the possibility of strong interactions with supported transition metals [6–11]. With the use of CeO₂ as a carrier of oxide and metal active component nanoparticles, the key factors determining the functional properties of the catalyst are the morphology and textural and structural properties of cerium dioxide, the catalyst composition, and the method and conditions of catalyst synthesis [11–15].

It was established [12–16] that the efficiency of supported metal nanoparticles in catalytic reactions depends on the morphology of CeO₂ support particles. In particular [12], the activity of RhPd/CeO₂ in the ethanol steam reforming (ESR) reaction increased in the following order: polycrystalline-structure CeO₂ < rod-shaped CeO₂ crystallites (CeO₂ rods) < cubic CeO₂ crystallites (CeO₂ cubes). According to Soykal et al. [15], the catalytic properties of Co/CeO₂ cube samples in ESR can be improved, as compared to those of Co/CeO₂ rod samples, due to both an increase in the dispersion and reducibility of the active component and a higher oxygen mobility in the CeO₂ crystal lattice. A similar dependence was observed for Ni catalysts in a decomposition reaction of N₂O, which was explained by a higher concentration of the Ce–O–Ni centers active in the reaction [16]. Sohn et al. [17] found that a difference in the reaction mechanisms of ESR, namely, the formation of formate or acetate intermediates in the presence of Co catalysts

based on micro- and nanoparticles of cerium dioxide, correlated with different concentrations of oxygen vacancies in the test samples.

It was found that an increase in the degree of metal–support interaction has a positive effect on the catalytic properties of materials based on CeO_2 [3, 9, 18–21]. For example, the activity of X– CeO_2 catalysts (X = Ru, Pd, and Pt) in the oxidation reactions of CO and CH_4 increased in the metal order $\text{Ru} < \text{Pd} < \text{Pt}$ due to an increase in the metal–cerium dioxide interaction observed in this order. It was noted [18, 19] that, in the case of a strong interaction between supported metal nanoparticles (clusters) and cerium dioxide, the transport of reactive oxygen species improved the resistance of the catalysts to coking. The doping of cerium dioxide [10, 20] and the varying of active component introduction methods [22–24] or catalyst heat treatment conditions [8, 25–27] were used in order to control the degree of metal– CeO_2 interactions. It was shown that the modification of cerium dioxide with lanthanum improved the dispersion of the Ni active component and the stability of catalyst operation in ethanol autothermal reforming (ATR) [10]. In contrast to impregnation and solvothermal decomposition, the use of an inverse emulsion method for the preparation of Co/ CeO_2 resulted in higher ESR process characteristics due to an increase in the dispersion of the active component and the formation of a developed metal–support interface. The ultimate variant of the strong interaction between the supported active component and the carrier is the formation of joint surface or bulk phases, for example, solid solutions with fluorite or perovskite structures and mixed oxides with a spinel structure. With the use of these materials as catalyst precursors, in some cases, their activation in a reducing or reaction atmosphere is required, which leads to the destruction of the initial joint phase and the formation of highly dispersed supported active component particles on the surface of the oxide carrier [28–31].

Thus, cerium dioxide–based catalysts are promising materials, which can be improved by the target-oriented regulation of the degree of metal–support interactions. In this work, in order to develop highly active and carbonization-resistant catalysts for hydrocarbon reforming, we synthesized and comprehensively studied (by low-temperature nitrogen adsorption, X-ray phase analysis, Raman spectroscopy, transmission electron microscopy, temperature-programmed reduction with hydrogen, and testing in autothermal ethanol reforming) Ni/ CeO_2 catalysts with different nickel contents (0–15 wt %). To optimize the form of stabilization, dispersion, and redox properties of the active component, the catalyst preparation methods (polymer ester precursor method and incipient wetness impregnation) were varied to provide different degrees of interaction between the Ni-containing active component and cerium dioxide.

This work continues a cycle of studies directed to the development of approaches to the control of the functional properties of catalysts through the regulation of their physicochemical characteristics [10, 20, 32–35].

EXPERIMENTAL

Catalyst Synthesis Procedures

The Ni/ CeO_2 catalysts were prepared by the polymer ester precursor method (P series) and incipient wetness impregnation (I series). For the synthesis of samples by the polymer ester precursor method, citric acid was dissolved in ethylene glycol at a temperature of 70°C. An aqueous solution with a given concentration of cerium nitrate and nickel nitrate (Ce + Ni) and ethylenediamine were sequentially added to the solution prepared. The molar ratio (Ce + Ni) : citric acid : ethylene glycol : ethylenediamine was 1 : 4 : 12 : 4. The resulting gel was stirred and then dried under an IR lamp for 72 h to remove excess solvent. The resulting resinous substance was calcined in a muffle furnace at a temperature of 500°C for 4 h.

To obtain catalyst samples by incipient wetness impregnation, the CeO_2 support, which was synthesized according to a published procedure [36], was impregnated with an aqueous solution of nickel nitrate with a given concentration; the samples were dried under an IR lamp and calcined in a muffle furnace at 500°C for 4 h.

In the designation of the samples, the numbers before Ni show its mass concentration in the catalyst (2, 5, 10, or 15 wt %). Before the reaction, the catalysts were activated in a flow of 30 vol % H_2/He at 600°C for one hour.

Physicochemical Methods for Catalyst Characterization

The metal content of the test catalysts was determined by X-ray fluorescence analysis on an ARL ADVANT'X analyzer (ThermoTechno Scientific, Switzerland) with an Rh anode of the X-ray tube.

The textural characteristics of the catalysts (specific surface area (S_{BET}), pore volume (V_{pore}), and average pore diameter (D_{pore}) were determined on an ASAP 2400 automated volumetric instrument (Micromeritics, the United States) by measuring and treating the isotherms of low-temperature nitrogen adsorption at 77 K.

The X-ray diffraction (XRD) analysis of the samples was performed on an HZG-4C diffractometer (Freiberger Präzisionmechanik, Germany) in monochromatic $\text{CoK}\alpha$ radiation ($\lambda = 1.79021 \text{ \AA}$). The phase composition was determined from diffraction patterns obtained by scanning the angle region $2\theta = 10^\circ\text{--}80^\circ$ with a step of 0.1 deg and an accumulation time of 6–15 s. The dimensions of coherent scattering regions (CSRs) of $\text{Ce}_{1-x}\text{Ni}_x\text{O}_y$ ($x = 0\text{--}0.4$) were calculated

from the 1.1.1. diffraction peak broadening of detected phases having a fluorite-type cubic structure; the CSRs of NiO and Ni were determined based on the 2.0.0. peak of a NiO phase and the 2.0.0. peak of a Ni⁰ phase, respectively.

The Raman spectra were measured in a spectral frequency shift range of 120–900 cm⁻¹ on a Renishaw Invia Raman spectrometer (Renishaw, the United Kingdom) using an argon laser with a wavelength of 514.5 nm as an excitation source, a 1800 l/mm diffraction grating, and an L50x lens. The laser radiation power on the sample did not exceed 2 mW, and the useful signal accumulation time was 30 s.

The high-resolution transmission electron microscopy (HR TEM) images were taken on a JEM–2010 electron microscope (JEOL, Japan) with a lattice resolution of 0.14 nm at an accelerating voltage of 200 kV. The local elemental analysis of the samples was carried out by energy-dispersive X-ray (EDX) spectrometry on an EDAX spectrometer (EDAX, the United States) equipped with a Si(Li) detector with an energy resolution of no less than 130 eV. The samples for HR TEM were supported onto perforated carbon substrates fixed on copper gauze.

Temperature-programmed reduction with hydrogen (TPR-H₂) was performed in a flow reactor (inner diameter, 5 mm) according to a procedure described elsewhere [37].

The thermal analysis (differential thermal analysis (DTA), thermogravimetric analysis (TGA), and differential thermogravimetric analysis (DTG)) of the samples was performed on a NETZSCH STA 449 C thermal analyzer (NETZSCH-Geratebau GmbH, Germany) in a temperature range of 25–900°C at a heating rate of 10 K/min in an atmosphere of air.

Methods for Studying the Activity of Catalysts

The activity of catalysts in the ATR reaction of ethanol was studied in a quartz flow reactor (inner diameter, 11 mm) according to a procedure described previously [10] at atmospheric pressure, a temperature of 200–600°C, a gas flow rate of 320 mL/min (NTP), and the reactant molar ratio C₂H₅OH : H₂O : O₂ : He = 1 : 3 : 0.4 : 0.7.

RESULTS AND DISCUSSION

Physicochemical Properties

Table 1 shows the textural and structural properties of the synthesized Ni/CeO₂ catalysts and the results of their study using the TPR-H₂ method. According to the X-ray fluorescence analysis data, the concentrations of metals in all of the samples were consistent with the calculated values. From the results of the study of the samples by the low-temperature adsorption of nitrogen, it follows that the method of synthesis

has a significant effect on the textural characteristics of the catalysts (Table 1). The specific surface area of samples from the P series was higher than that of samples from the I series. This effect increased with the fraction of nickel in the catalyst (Table 1). Thus, at a 2 wt % Ni content of Ni/CeO₂ (P) and Ni/CeO₂ (I) samples, $S_{\text{BET}} = 105$ and 85 m²/g, respectively, or $S_{\text{BET}} = 115$ and 65 m²/g, respectively, as the nickel concentration was increased to 15 wt %. Note that the S_{BET} of P-series catalysts varied only slightly with the nickel content and reached 110 ± 5 m²/g, which is higher than that of similar systems obtained by a hydrothermal method [38]. On the contrary, for I-series catalysts, the specific surface area decreased from 85 to 65 m²/g with an increase in the fraction of Ni; this can be due to the partial blocking of support pores with active component crystallites [37]. Regardless of the method of synthesis, the Ni/CeO₂ catalysts were mesoporous materials, as indicated by their type IV adsorption isotherms with an H3 hysteresis loop.

An analysis of Ni/CeO₂ diffraction patterns showed that the phase composition of the samples depended on their preparation methods (Fig. 1). According to the XRD analysis data, the P-series samples were single-phase, and they consisted of a cerium dioxide phase. The absence of peaks related to Ni-containing phases can indicate the stabilization of nickel cations as a constituent of either solid solution based on cerium dioxide or finely dispersed nickel oxide particles (CSR < 4 nm). The formation of a Ce_{1-x}Ni_xO_y solid solution could be indicated by a change in the CeO₂ unit cell parameter. As a rule, the replacement of cerium cations ($r_{\text{Ce}^{4+}} = 0.097$ nm) by cations with a smaller radius (in particular, $r_{\text{Ni}^{2+}} = 0.081$ nm) is accompanied by a decrease in the cell parameter and a shift of diffraction peaks to larger angles [36, 38]. However, regardless of the catalyst synthesis method and the nickel content of the catalyst, the cerium dioxide cell parameter (5.413 ± 0.002 Å) remained unchanged upon the introduction of an active component into the carrier matrix. The I-series samples were two-phase: a NiO active component phase was present in addition to the support phase.

The estimation of the average size of crystalline domains (the size of a coherent scattering region) using the Scherrer equation showed that the CSR size (CeO₂) decreases from 11.0 to 5.5 nm as the nickel content of the P-series samples was increased from 0 to 15 wt %, whereas it remained unchanged (11.0 nm) in the case of the I series. The observed decrease in the CSR (CeO₂) in Ni/CeO₂ (P) samples, which were obtained by the polymer ester precursor method, was similar to the effect observed upon the doping of cerium dioxide with La, Gd, or Mg cations [36]. In particular, Kerzhentsev et al. [40] found that an increase in the mole fraction of a doping cation from 0.1 to 0.9 led to a decrease in the average size of CeO₂

Table 1. Physicochemical properties of the support and catalysts

Sample	Texture characteristics			XRD data						Raman-spectroscopic data	Results of TPR-H ₂	
	S _{BET} , m ² /g	V _{pore} , cm ³ /g	D _{pore} , nm	after calcination*			after activation**				I ₅₇₀ /I ₄₆₅	(mmolH ₂)/g _{Cat}
				phase composition	CSR size of CeO ₂ , nm	CSR size of NiO, nm	phase composition	CSR size of CeO ₂ , nm	CSR size of Ni ²⁺ , nm			
CeO ₂	85	0.20	9.6	CeO ₂	11.0	–	CeO ₂	25	–	0	1.13	0
Unmodified cerium dioxide												
Catalysts prepared by the polymer ester precursor method												
2Ni/CeO ₂ (P)	105	0.20	7.3	CeO ₂	8.0	–	CeO ₂	19.0	–	0.42	1.23	0.29
5Ni/CeO ₂ (P)	110	0.24	8.5	CeO ₂	6.5	–	CeO ₂ , Ni	19.0	6.0	0.61	1.29	0.19
10Ni/CeO ₂ (P)	105	0.23	8.8	CeO ₂	5.5	–	CeO ₂ , Ni	18.0	7.8	1.03	2.37	0.73
15Ni/CeO ₂ (P)	115	0.27	9.1	CeO ₂	5.5	–	CeO ₂ , Ni	14.0	8.2	1.39	2.98	0.73
Catalysts prepared by incipient wetness impregnation												
2Ni/CeO ₂ (I)	85	0.22	9.9	CeO ₂	11.0	–	CeO ₂	25.0	–	0.06	1.26	0.38
5Ni/CeO ₂ (I)	80	0.19	9.6	CeO ₂ , NiO	11.0	20.0	CeO ₂ , Ni	25.0	20.0	0.24	1.62	0.58
10Ni/CeO ₂ (I)	75	0.19	10.1	CeO ₂ , NiO	11.0	25.0	CeO ₂ , Ni	25.0	25.0	0.14	2.92	1.06
15Ni/CeO ₂ (I)	65	0.16	9.7	CeO ₂ , NiO	11.0	50.0	CeO ₂ , Ni	25.0	50.0	0.12	3.61	0.98

* Samples after calcination at 500°C in air.

** Samples after reduction at 600°C in a mixture of 30% H₂/He.

Dashes indicate the absence of the characteristic (the CSR size of NiO/Ni) for these samples due to the absence of NiO/Ni phases, as can be evident from the phase composition of the samples.

crystallites from 12 to 3 nm. A decrease in the size of CSRs upon doping is a widely known phenomenon for the CeO₂ system caused by the inhibition of crystallite growth in the presence of a doping cation [41]. Note that the cell parameter increased from 5.41 to 5.54 Å upon a decrease in the particle size of unmodified CeO₂ from 70 to 2.8 nm [42]. In this regard, the absence of an effect of the introduced nickel cation on the CeO₂ cell parameter in the P-series samples can be due to a decrease in the size of CeO₂ crystallites. Accordingly, it can be assumed that, during the synthesis of Ni/CeO₂ (P), a portion of nickel was included into the solid solution based on cerium dioxide; this led to an observed decrease in crystallite sizes and to an increase in the specific surface area of samples, as compared to those of unmodified cerium dioxide. This indicates an increase in the sintering resistance of the structure of P-series samples in comparison with those of the structures of the initial CeO₂ support and the I-series samples.

It is well known that the nonisovalent replacement of cerium cations with Ni²⁺ cations leads to the disruption of oxygen stoichiometry and, consequently, an increase in the defect structure of the material [43–45]. Indeed, an analysis of the Raman spectroscopy data (Fig. 2, Table 1) showed that the structure imperfection of materials related to the presence of oxygen vacancies increased in the following order: CeO₂ < Ni/CeO₂ (I) < Ni/CeO₂ (P). This was confirmed by (1) the presence of Raman scattering bands in a region of 550–650 cm⁻¹, which appeared upon doping cerium dioxide with metal cations of a different radius and valence; (2) the values of a I_{570}/I_{466} band intensity ratio, which is used to evaluate the defect structure of CeO₂; and (3) an increase in the Raman scattering band intensity at 220–230 cm⁻¹ due to transverse acoustic vibrations [43–45]. In particular, it can be seen (Table 1) that the parameter I_{570}/I_{466} for the P-series samples (0.4–1.4) was significantly higher than that for the I-series samples (0.1–0.2). In addition, in contrast to Ni/CeO₂ (I), the value of I_{570}/I_{466} for Ni/CeO₂ (P) increased from 0.4 to 1.4 as the Ni content of the catalyst was increased from 2 to 15 wt %, and the maximum position of the F_{2g} mode of CeO₂ (466 cm⁻¹) shifted toward lower frequencies by 14 cm⁻¹. The observed effects can be due to the partial replacement of cerium cations by nickel cations and the formation of the Ce_{1-x}Ni_xO_y solid solution [43–45].

The results of the TEM analysis of the samples (Fig. 3) are in good agreement with the XRD analysis and Raman spectroscopy data. It was established that cerium dioxide particles were crystallites ~10 nm in size, which formed polycrystalline agglomerates mainly in the form of plates. In the I-series samples, nickel oxide particles were observed on the support surface; the range of sizes of these particles depended on the nickel content: from 3 to 10 nm for 2Ni/CeO₂

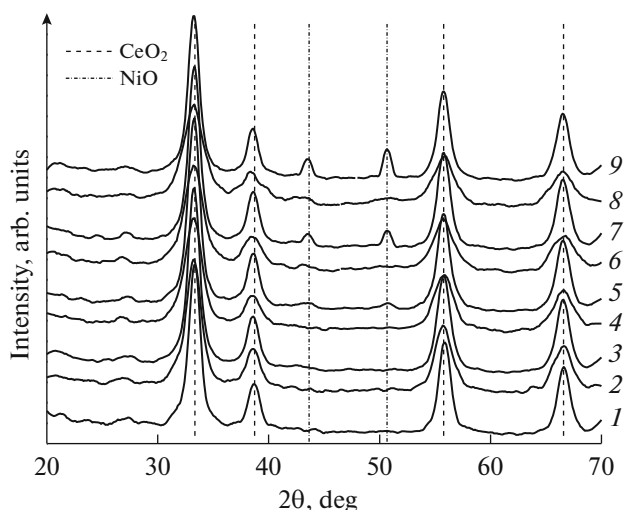


Fig. 1. Effect of the preparation method on the phase composition of the Ni/CeO₂ catalysts: (1) CeO₂, (2) 2Ni/CeO₂ (P), (3) 2Ni/CeO₂ (I), (4) 5Ni/CeO₂ (P), (5) 5Ni/CeO₂ (I), (6) 10Ni/CeO₂ (P), (7) 10Ni/CeO₂ (I), (8) 15Ni/CeO₂ (P), and (9) 15Ni/CeO₂ (I).

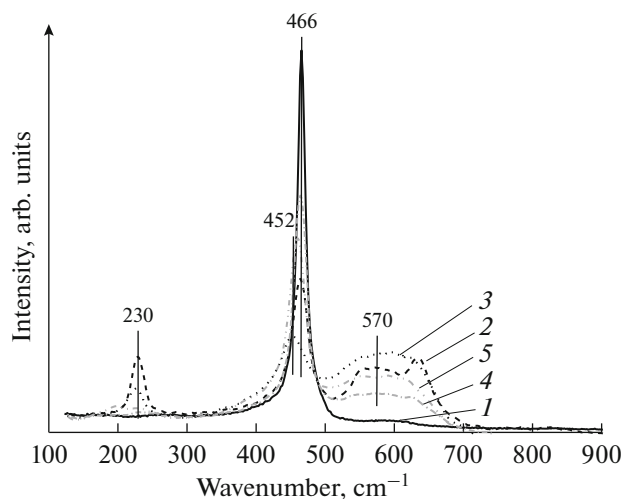


Fig. 2. Raman spectra of (1) the support and the Ni/CeO₂ catalysts: (2) 2Ni/CeO₂ (P), (3) 15Ni/CeO₂ (P), (4) 2Ni/CeO₂ (I), and (5) 15Ni/CeO₂ (I).

(I) or from 3 to 30 nm for 10Ni/CeO₂ (I) (Fig. 3b). The Ni/CeO₂ (P) samples were formed by crystallites with characteristic sizes to 8 nm; their structure was highly defective, and nickel oxide particles were almost not observed with the exception of single particles smaller than 5 nm in the samples with a high nickel content (10–15 wt %) (Fig. 3a).

Because catalysts were activated by reduction before the ethanol ATR reaction for the formation of the active component, namely, Ni⁰, the phase composition of the samples after activation at 600°C in 30% H₂/He was studied and the characteristics of their

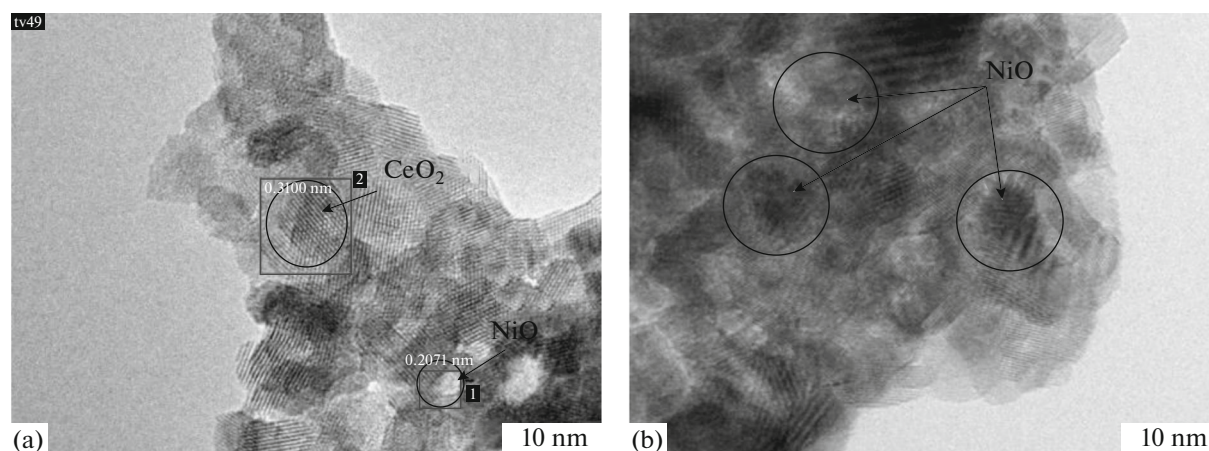
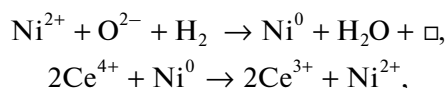


Fig. 3. HR TEM micrographs of (a) 10Ni/CeO₂ (P) and (b) 10Ni/CeO₂ (I) catalysts.

reduction under TPR-H₂ conditions were determined (Table 1). Table 1 indicates that, despite the high-temperature treatment in a reducing atmosphere, the P-series catalysts, unlike the I-series samples, retained the high dispersion of both the support (14–19 nm versus 25 nm) and the active component (6–8 nm against 20–50 nm).

Figure 4 shows TPR-H₂ curves for the Ni/CeO₂ (P) and Ni/CeO₂ (I) samples with different nickel contents. In the TPR-H₂ curves of unmodified cerium dioxide, two hydrogen consumption regions can be distinguished in temperature ranges of 100–600°C (a peak maximum at $T = 510^\circ\text{C}$) and 600–1000°C (a peak maximum at $T = 880^\circ\text{C}$) due to the reduction of Ce⁴⁺ cations localized on the surface and in the bulk of the particles, respectively [46]. The introduction of nickel into the support matrix changed the profile of TPR-H₂ curves mainly in a low-temperature region ($T < 600^\circ\text{C}$). In the case of the P-series catalysts, in addition to a peak with a maximum at 880°C, there were two peaks with maximums at ~ 160 and $230 \pm 5^\circ\text{C}$ and a broad peak at 250–450°C without a pronounced maximum (Fig. 4a). In the case of the I-series samples, the presence of Ni in their composition led to the appearance of two peaks with maximums at 235 ± 10 and $340 \pm 20^\circ\text{C}$ (Fig. 4b). Regardless of the preparation method, the position and intensity of peaks at $T < 250^\circ\text{C}$ remained unchanged as the nickel content was increased from 2 to 15 wt %, whereas the consumption intensity at 250–450°C increased (Fig. 4). According to an analysis of the literature data [47–49], the following three regions of hydrogen consumption can be distinguished for the Ni–Ce–O materials: low-temperature ($T < 250^\circ\text{C}$), medium ($250^\circ\text{C} < T < 550^\circ\text{C}$), and high-temperature ($T > 550^\circ\text{C}$) regions. The first region of H₂ consumption was due to the presence of [Ni–O–Ce] structures localized on the surface of a solid solution or at the points of contact of highly dispersed nickel oxide particles with cerium dioxide crys-

tallites. Lamonier et al. [47] proposed the following reduction scheme, in which nickel metal (initially formed from Ni²⁺ cations) promotes the reduction of surface Ce⁴⁺ cations to Ce³⁺ to become reoxidized to Ni²⁺:



where \square is an oxygen vacancy.

The consumption of H₂ at $250 < T < 550^\circ\text{C}$ is related to the reduction of nickel cations as the constituents of particles, nickel oxide clusters, and solid solution. An increase in the Ni²⁺ reduction temperature can be caused by (1) an increase in the degree of metal–support interaction and (2) the formation of large nickel oxide particles [47–49]. Lamonier et al. [47] noted that, on the formation of a Ce_{1-x}M_xO_y solid solution (M = Cu or Ni), the reducibility of Ce⁴⁺ cations increased and that of Mⁿ⁺ decreased, as compared with the corresponding single-component oxides. The third region of hydrogen consumption was related to the reduction of Ce⁴⁺ cations localized in the bulk of the particles. In accordance with the above and based on the experimental TPR-H₂ data for the samples of P and I series (Fig. 4), we can conclude that the contact area between the active component and the support was more developed and the range of stabilized nickel cation species was wider when the polymer ester precursor method was used. Moreover, lower values of both total hydrogen consumption and H₂/Ni ratios for the P-series samples, as compared with those of the I-series samples, are indicative of a lower reducibility of the systems obtained by the polymer ester precursor method; this can be due to the formation of the Ce_{1-x}Ni_xO_y solid solution.

To establish a synthesis method–structure–properties relationship, we tested the catalysts obtained in the autothermal reforming reaction of ethanol.

Activity of the Catalysts in the Autothermal Reforming of Ethanol

Table 2 summarizes the results of a study of the activity of the support and Ni/CeO₂ catalysts in the ATR reaction of ethanol. In addition to hydrogen, a wide range of C-containing products was formed: carbon oxides, methane, ethylene, acetaldehyde, and acetone. Regardless of the catalyst composition and preparation method, an increase in the conversion of ethanol and the yield of hydrogen with reaction temperature was observed; selectivity for the formation of carbon monoxide increased, and selectivity for the formation of C₂–C₃ by-products decreased. This is consistent with previously obtained data and reflects the features of the mechanism of this reaction [50].

As follows from the data of Table 2, the yield of hydrogen was no higher than 20% in the presence of CeO₂. The introduction of nickel led to an improvement in the process performance characteristics: the conversion of ethanol and the yield of hydrogen increased, while the yield of C₂–C₃ by-products decreased (Table 2). As the nickel content of the P-series was increased from 2 to 15 wt %, the yield of hydrogen increased from 35 to 55%, whereas it remained almost unchanged (40–45%) for the I series. For all of the Ni/CeO₂ test samples, the process parameters remained almost unchanged in the course of reaction for 6 h. However, in the presence of CeO₂, the conversion of ethanol decreased from 100 to 70%.

To assess the degree of carbonization of catalysts in the course of the autothermal reforming of ethanol, the catalysts were studied 6 h after the ATR reaction of ethanol (reaction temperature, 600°C) by thermal analysis in an atmosphere of air. It was established (Table 2) that the amount of carbon deposits depends on the composition and preparation method of Ni/CeO₂. In the case of the P-series samples, the fraction of carbon deposits was 3–4 wt %, and it changed only slightly upon varying the sample composition. For the I-series samples, the amount of carbon deposits increased significantly from ~3 to 30% as the nickel content was increased from 2 to 15 wt %. Therefore, the catalysts obtained by the polymer ester precursor method were characterized by high resistance to the formation of carbon deposits in contrast to the samples prepared by impregnation.

It is reasonable that differences in the functional properties of the samples are due to their different physicochemical characteristics. As shown above, the method of preparation is responsible for the textural and structural properties of these materials and for their reducibility. As compared with the I-series samples, the P-series Ni/CeO₂ catalysts were characterized by different forms of stabilization of the active component (a Ce_{1-x}Ni_xO_y solid solution phase and NiO particles of size <5 nm against a NiO phase with a particle size of 5–50 nm), a smaller average CeO₂

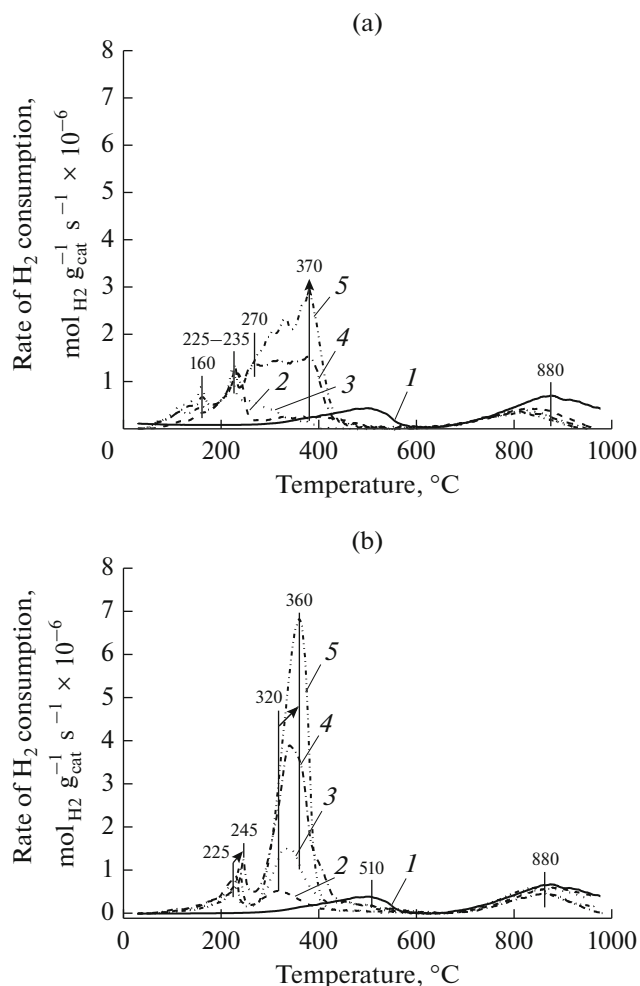


Fig. 4. Effect of the preparation method on the TPR-H₂ of Ni/CeO₂ catalysts: (a) P-series and (b) I series. Ni contents, wt %: (1) 0, (2) 2, (3) 5, (4) 10, and (5) 15.

crystallite size (5–8 against 11 nm), a higher specific surface area (105–115 against 65–85 m²/g), and a defect structure but lower reducibility. It is likely that the observed differences resulted from the partial incorporation of nickel cations into the crystal lattice of cerium dioxide and the formation of the Ce_{1-x}Ni_xO_y solid solution. It is important to note that, as a result of reductive activation, the highly dispersed Ni⁰ active phase particles were formed in Ni/CeO₂ (P) samples, unlike the I-series catalysts: these particles were characterized by a high dispersion of the active component (6–8 nm against 20–50 nm). It is well known that the rate of formation of carbon deposits decreases with decreasing Ni⁰ particle size [51], and the stable growth of fibrous carbon occurs on particles of sizes 20–60 nm [52]. The high dispersion of the active component also causes a developed metal–support contact surface, which facilitates the efficient transport of reactive oxygen species from the support to C-containing intermediates formed at the Ni centers. A higher concentra-

Table 2. Activity* of the support and catalysts in the autothermal reforming reaction of ethanol and the degree of their carbonization

Sample	T, °C	$X_{C_2H_5OH}$, %	Y_{H_2} , %	S, %						C**, %
				CO	CO ₂	CH ₄	C ₂ H ₄	C ₂ H ₄ O	C ₃ H ₆ O	
CeO ₂	300	42	5	4	36	1	19	18	22	1.7
	400	72	9	6	31	3	21	8	31	
	500	88	15	6	30	6	14	6	38	
	600	99	22	16	41	20	11	4	8	
2Ni/CeO ₂ (P)	300	26	5	3	52	1	4	19	21	3.6
	400	54	12	6	45	1	4	33	11	
	500	58	20	17	41	6	1	26	9	
	600	97	35	30	46	11	1	9	2	
2Ni/CeO ₂ (I)	300	56	15	10	46	4	6	5	29	2.9
	400	78	24	11	40	4	5	8	32	
	500	88	30	18	41	5	5	5	26	
	600	99	42	23	63	11	0	2	1	
15Ni/CeO ₂ (P)	300	99	20	1	56	42	1	0	0	3.1
	400	100	25	3	63	34	0	0	0	
	500	100	40	10	63	27	0	0	0	
	600	100	54	27	61	12	0	0	0	
15Ni/CeO ₂ (I)	300	83	17	18	38	25	2	13	4	33.8
	400	99	21	5	63	31	0	1	0	
	500	99	32	9	63	26	0	1	1	
	600	100	40	23	59	18	0	0	0	

* Ethanol conversion ($X_{C_2H_5OH}$), yield of hydrogen (Y_{H_2}), and selectivity for product formation (S).

** The amount of carbon deposits in the catalysts after 6 h of the ATR reaction of ethanol at 600°C according to the results of thermal analysis.

tion of oxygen vacancies in the P-series samples affects the oxygen capacity of the material and the mobility of oxygen and, hence, the efficiency of the removal of carbon deposits [45, 53]. Thus, we can conclude that the polymer ester precursor method ensures a strong metal–support interaction, which leads to the resistance of the active component against agglomeration and its stabilization in a highly dispersed state. As a consequence, the P-series catalysts exhibit high resistance to carbonization during the catalytic process.

CONCLUSIONS

We systematically studied the physicochemical and catalytic properties of Ni/CeO₂ (2, 5, 10, and 15 wt %) depending on the method of their synthesis (the polymer ester precursor method or incipient wetness impregnation). We established that the best way to prepare Ni/CeO₂ is the polymer ester precursor method. In contrast to impregnation, with the use of

this method, the Ni active component was stabilized in a highly dispersed state, which ensured its resistance to the formation of carbon deposits in the course of the autothermal reforming of ethanol.

ACKNOWLEDGMENTS

We are grateful to I.L. Kraevskaya, T.Ya. Efimenko, G.S. Litvak, and Cand. Sci. (Chem.) E.Yu. Gerasimov for their assistance in the study of the samples by physicochemical methods.

This work was supported by the Russian Foundation for Basic Research (project no. 18-53-45012 IND_a).

REFERENCES

1. Ismagilov, Z.R., Kuznetsov, V.V., Okhlopko, L.B., Tsikoza, L.T., and Yashnik, S.A., *Oksidy titana, tseriya, tsirkoniya, itriya, alyuminiya. Svoystva, primeneniye i metody polucheniya* (Titanium, Cerium, Zirconium,

- Yttrium, Zluminum Oxides. Properties, Application, and Methods of Synthesis), Novosibirsk: Izdatel'stvo SO RAN, 2010.
- Paier, J., Penschke, C., and Sauer, J., *Chem. Rev.*, 2013, vol. 113, p. 3949.
 - Rodriguez, J.A., Grinter, D.C., Liu, Z., Palomino, R.M., and Senanayake, S.D., *Chem. Soc. Rev.*, 2017, vol. 46, p. 1824.
 - Kuznetsova, T.G. and Sadykov, V.A., *Kinet. Catal.*, 2008, vol. 49, no. 6, p. 840.
 - Ivanov, V.K., Polezhaeva, O.S., and Tret'yakov, Yu.D., *Russ. J. Gen. Chem.*, 2010, vol. 80, p. 604.
 - Ismagilov, I.Z., Matus, E.V., Kuznetsov, V.V., Mota, N., Navarro, R.M., Kerzhentsev, M.A., Ismagilov, Z.R., and Fierro, J.L.G., *Catal. Today*, 2013, vol. 210, p. 10.
 - Wang, F., Wei, M., Evans, D.G., and Duan, X., *J. Mater. Chem. A*, 2016, vol. 4, p. 5773.
 - Gonzalez-DelaCruz, V.M., Holgado, J.P., Pereñíguez, R., and Caballero, A., *J. Catal.*, 2008, vol. 257, p. 307.
 - Malyutin, A.V., Mikhailichenko, A.I., Zubavichus, Ya.V., Murzin, V.Yu., Koshkin, A.G., and Sokolov, I.V., *Kinet. Catal.*, 2015, vol. 56, no. 1, p. 89.
 - Ismagilov, Z.R., Matus, E.V., Ismagilov, I.Z., Sukhova, O.B., Yashnik, S.A., Ushakov, V.A., and Kerzhentsev, M.A., *Catal. Today*, 2019, vol. 323, p. 166.
 - Capdevila-Cortada, M., Vilé, G., Teschner, D., Pérez-Ramírez, J., and López, N., *Appl. Catal., B*, 2016, vol. 197, p. 299.
 - Divins, N.J., Casanovas, A., Xu, W., Senanayake, S.D., Wiater, D., Trovarelli, A., and Llorca, J., *Catal. Today*, 2015, vol. 253, p. 99.
 - Hong, W., Lijuan, Z., Miao, L., Yuan, L., and Xue, B., *J. Rare Earths*, 2013, vol. 31, no. 6, p. 565.
 - Cai, W., Wang, F., Daniel, C., van Veen, A.C., Schuurman, Y., Descorme, C., Provendier, H. Shen, W., and Mirodatos, C., *J. Catal.*, 2012, vol. 286, p. 137.
 - Soykal, I.I., Bayram, B., Sohn, H., Gawade, P., Miller, J.T., and Ozkan, U.S., *Appl. Catal., A*, 2012, vol. 449, p. 47.
 - Zhao, P., Qin, F., Huang, Z., Sun, C., Shen, W., and Xu, H., *Catal. Sci. Technol.*, 2018, vol. 8, p. 276.
 - Sohn, H., Celik, G., Gunduz, S., Dogu, D., Zhang, S., Shan, J., Tao, F.F., and Ozkan, U.S., *Catal. Lett.*, 2017, vol. 147, p. 2863.
 - Liu, Z., Duchoň, T., Wang, H., Peterson, E.W., Zhou, Y., Luo, S., Zhou, J., Matolín, V., Stacchiola, D.J., Rodriguez, J.A., and Senanayake, S.D., *J. Phys. Chem.*, 2015, vol. 119, p. 18248.
 - Liu, Z., Duchon, T., Wang, H., Grinter, D.C., Waluyo, I., Zhou, J., Liu, Q., Jeong, B., Crumlin, E.J., Matolin, V., Stacchiola, D.J., Rodriguez, J.A., and Senanayake, S.D., *Phys. Chem. Chem. Phys.*, 2016, vol. 18, p. 16621.
 - Matus, E.V., Nefedova, D.V., Kuznetsov, V.V., Ushakov, V.A., Stonkus, O.A., Ismagilov, I.Z., Kerzhentsev, M.A., and Ismagilov, Z.R., *Kinet. Catal.*, 2017, vol. 58, no. 5, p. 623.
 - Cai, W., Wanga, F., Zhan, E., Van Veen, A.C., Mirodatos, C., and Shen, W., *J. Catal.*, 2008, vol. 257, p. 96.
 - Song, H., Tan, B., and Ozkan, U.S., *Catal. Lett.*, 2009, vol. 132, p. 422.
 - Liu, Z., Senanayake, S.D., and Rodriguez, J.A., *Appl. Catal., B*, 2016, vol. 197, p. 184.
 - Carvalho, F.L.S., Asencios, Y.J.O., Bellido, J.D.A., and Assaf, E.M., *Fuel Process. Technol.*, 2016, vol. 142, p. 182.
 - Soykal, I.I., Sohn, H., Miller, J.T., and Ozkan, U.S., *Top. Catal.*, 2014, vol. 57, p. 785.
 - Bayram, B., Soykal, I.I., von Deak, D., Miller, J.T., and Ozkan, U.S., *J. Catal.*, 2011, vol. 284, p. 77.
 - Matus, E.V., Okhlopko, L.B., Sukhova, O.B., Ismagilov, I.Z., Kerzhentsev, M.A., and Ismagilov, Z.R., *J. Nanopart. Res.*, 2019, vol. 21, p. 11.
 - Wang, M., Zhao, T., Li, M., and Wang, H., *RSC Adv.*, 2017, vol. 7, p. 41847.
 - Ismagilov, I.Z., Matus, E.V., Kuznetsov, V.V., Yashnik, S.A., Prosvirin, I.P., Kerzhentsev, M.A., Ismagilov, Z.R., Mota, N., Navarro, R.M., and Fierro, J.L.G., *Appl. Catal., A*, 2014, vol. 481, p. 104.
 - Mota, N., Ismagilov, I.Z., Matus, E.V., Kuznetsov, V.V., Kerzhentsev, M.A., Ismagilov, Z.R., Navarro, R.M., and Fierro, J.L.G., *Int. J. Hydrogen Energy*, 2016, vol. 41, p. 19373.
 - Zhang, L., Wang, X., Chen, C., Zou, X., Shang, X., Ding, W., and Lu, X., *RSC Adv.*, 2017, vol. 7, p. 33143.
 - Ismagilov, I.Z., Matus, E.V., Kuznetsov, V.V., Kerzhentsev, M.A., Yashnik, S.A., Prosvirin, I.P., Mota, N., Navarro, R.M., Fierro, J.L.G., and Ismagilov, Z.R., *Int. J. Hydrogen Energy*, 2014, vol. 39, p. 20992.
 - Ismagilov, I.Z., Matus, E.V., Popkova, V.S., Kuznetsov, V.V., and Ushakov, V.A., Yashnik, S.A., Prosvirin, I.P., Kerzhentsev, M.A., and Ismagilov, Z.R., *Kinet. Catal.*, 2017, vol. 58, no. 5, p. 622.
 - Ismagilov, I.Z., Matus, E.V., Kuznetsov, V.V., Kerzhentsev, M.A., Yashnik, S.A., Larina, T.V., Prosvirin, I.P., Navarro, R.M., Fierro, J.L.G., Gerritsen, G., Abbenhuis, H.C., Ismagilov, Z.R., *Eurasian Chem. Technol. J.*, 2016, vol. 18, no. 2, p. 93.
 - Ismagilov, I.Z., Matus, E.V., Kuznetsov, V.V., Yashnik, S.A., Kerzhentsev, M.A., Gerritsen, G., Abbenhuis, H.C., Ismagilov, Z.R., *Eurasian Chem. Technol. J.*, 2017, vol. 19, no. 1, p. 3.
 - Kerzhentsev, M.A., Matus, E.V., Ismagilov, I.Z., Ushakov, V.A., Stonkus, O.A., Larina, T.V., Kozlova, G.S., Bharali, P., and Ismagilov, Z.R., *J. Struct. Chem.*, 2017, vol. 58, no. 1, p. 126.
 - Ismagilov, I.Z., Matus, E.V., Nefedova, D.V., Kuznetsov, V.V., Yashnik, S.A., Kerzhentsev, M.A., and Ismagilov, Z.R., *Kinet. Catal.*, 2015, vol. 56, no. 3, p. 394.
 - Hu, Z., Qiu, S., You, Y., Guo, Y., Guo, Y., Wang, L., Zhan, W., and Lu, G., *Appl. Catal., B*, 2018, vol. 225, p. 110.
 - Katta, L., Sudarsanam, P., Thrimurthulu, G., and Reddy, B.M., *Appl. Catal., A*, 2010, vol. 101, p. 101.
 - Kerzhentsev, M.A., Matus, E.V., Ismagilov, I.Z., Sukhova, O.B., Bharali, P., and Ismagilov, Z.R., *Eurasian Chem. Technol. J.*, 2018, vol. 20, p. 283.
 - Ponchel, A., D'Huysser, A., Lamonier, C., and Jalowiecki-Duhamel, L., *Phys. Chem. Chem. Phys.*, 2000, vol. 2, p. 303.

42. Wu, L., Wiesmann, H.J., Moodenbaugh, A.R., Klie, R.F., Zhu, Y., Welch, D.O., and Suenaga, M., *Phys. Rev. B*, 2014, vol. 69, p. 125415.
43. Romero-Nunez, A. and Diaz, G., *RSC Adv.*, 2015, vol. 5, p. 54571.
44. Liyanage, A.D., Perera, S.D., Tan, K., Chabal, Y., and Balkus, K.J., *ACS Catal.*, 2014, vol. 4, p. 577.
45. Deng, J., Chu, W., Wang, B., Yanga, W., and Zhao, X.S., *Catal. Sci. Technol.*, 2016, vol. 46, p. 851.
46. Yu, Q., Wu, X., Tang, C., Qi, L., Liu, B., Gao, F., Sun, K., Dong, L., and Chen, Y., *J. Colloid Interface Sci.*, 2011, vol. 354, p. 341.
47. Lamonier, C., Ponchel, A., D'Huysser, A., and Jalowiecki-Duhamel, L., *Catal. Today*, 1999, vol. 50, p. 247.
48. Vita, A., Italiano, C., Fabiano, C., Lagana, M., and Pino, L., *Mater. Chem. Phys.*, 2015, vol. 163, p. 337.
49. Shan, W., Luo, M., Ying, P., Shen, W., and Li, C., *Appl. Catal., A*, 2003, vol. 246, p. 1.
50. Santos, J.B.O., Damyanova, S., Gallo, J.M.R., and Bueno, J.M.C., *ACS Catal.*, 2015, vol. 5, p. 3841.
51. Aramouni, N.A.K., Zeaiter, J., Kwapinski, W., and Ahmad, M.N., *Energy Convers. Manage.*, 2017, vol. 150, p. 614.
52. Christensen, K.O., Chen, D., Lødeng, R., and Holmen, A., *Appl. Catal.*, 2006, vol. 314, p. 9.
53. Vinodkumar, T., Rao, B.G., and Reddy, B.M., *Catal. Today*, 2015, vol. 253, p. 57.

Translated by V. Makhlyarchuk